Metallogr. Microstruct. Anal. (2016) 5:402–410
DOI 10.1007/s13632-016-0304-y

TECHNICAL ARTICLE

Effects of Applied Stress on Isothermal Phase Transformation of Austenite to Pearlite in Heavy Rail Steels: An Experimental and Modeling Study

Lin Chen[1] · Kunyu Chen[1] · Guo Chang[1] · Yuyan Liu[1]

Received: 3 April 2016 / Revised: 13 July 2016 / Accepted: 10 August 2016 / Published online: 14 September 2016

Abstract Recently, high-speed train systems are developing rapidly throughout the world. The heavy rail steel for the high-speed train needs to be heat treated after hot rolling, in order to improve its mechanical performances and to meet engineering requirements. This study aims at effects of applied stress on isothermal phase transformation of austenite to pearlite in heavy rail steels during heat treatment. Transformation kinetics and transformation plasticity models for isothermal phase transformations in the heavy rail steel have been established. The effects of stress on transformation kinetics and transformation plasticity have been analyzed. Also, the effects of stress on the morphology of the generated pearlite microstructure have been observed by confocal laser scanning microscopy and scanning electron microscopy. The results show that stress can speed up the transformation of austenite to pearlite. And, with increasing stress, the interlamellar spacing of lamellar pearlite decreases and the fraction of globular pearlite (exhibiting very short, globular-shaped lamellae) increases.

Keywords Phase transformation · Pearlite · Kinetics · Transformation plasticity

Abbreviations

T	Temperature (°C)
ε_r	Radial strain
$\varepsilon_{r\max}$	Maximum value of radial strain
d_0	Initial diameter (mm)
t	Time consumed for phase transformation of austenite to pearlite (s)
b	Microstructural evolution rate coefficient
K	Transformation plasticity coefficient
$\varepsilon_a^{\mathrm{tp}}$	Transformation plasticity strain in axial direction
$\varepsilon_a^{\mathrm{tr}}$	Transformation strain in axial direction
ε_r^e	Elastic strain in radial direction
β_P^T	Transformation coefficient at the temperature of T
$\varepsilon_{a,0}^e$	Elastic strain in axial direction in the initial state of the transformation
$\varepsilon_{a,f}^e$	Elastic strain in axial direction at the end of the transformation
E	Elasticity modulus of the studied steel (GPa)
σ	Stress (MPa)
ε_a	Axial strain
Δd	Variation of diameter during the phase transformation process (mm)
τ_s	Incubation time of phase transformation of austenite to pearlite (s)
f	Volume fraction of pearlite
n	Microstructural evolution rate coefficient
$\varepsilon_r^{\mathrm{tp}}$	Transformation plasticity strain in radial direction
$\varepsilon_r^{\mathrm{tr}}$	Transformation strain in radial direction
$\varepsilon_r^{\mathrm{th}}$	Thermal strain in radial direction
$\varepsilon_r^{e/}$	Corrected value of elastic strain in radial direction
υ	Poisson's ratio, $\upsilon = 0.5$
E_A	Elasticity modulus of austenite (GPa)
E_P	Elasticity modulus of pearlite (GPa)
$\Delta\varepsilon_a^e$	Variation of elastic strain in axial direction during the phase transformation process

✉ Lin Chen
chenlin39805@163.com

[1] School of Materials and Metallurgy, Inner Mongolia University of Science and Technology, Baotou 014010, People's Republic of China

Introduction

As an important method of altering and improving mechanical performances of metallic materials, heat treatment is widely used in manufacturing industry. However, on the basis of present technology, there are still great difficulties conducting trim-size heat treatment experiments on certain workpieces to design and optimize the heat treatment processes. Such experiments not only cannot achieve desired results, but also waste a lot of human effort, material, finances, and time. Traditional heat treatment technology is unable to accurately predict production results, and the determination of the heat treatment process depends greatly on experiences. Obviously, this is an obstacle to precisely controlling the quality of the heat-treated products and is a bottleneck of the development of metal manufacturing industry. Fortunately, however, with the advanced computer technology, numerical simulation becomes a powerful tool to study the heat treatment process. On the basis of numerical simulation, heat treatment experiments can be easily conducted in virtual laboratories. This enables the precise determination of the heat treatment process [1–3].

In the subject heat treatment process, phase transformations are usually accompanied by an applied stress which is lower than the yield stress of the material at the transformation temperature. The effects of the applied stress on the phase transformation process can be divided into two aspects: (1) stress-induced transformation, the effects of stress on phase transformation kinetics [4–6]; (2) transformation-induced plasticity, the effects of stress on mechanical behavior of the material. The transformation plasticity strain refers to the plastic strain during the transformation process with an applied stress lower than the yield stress [7–9]. The models of phase transformation kinetics and transformation plasticity are indispensable in the numerical simulation of heat treatment process, and the accurate models are the basic premises for the success of simulation. In order to improve the accuracy of the numerical simulation of the heat treatment process, it is necessary to accurately establish the transformation plasticity and kinetic models, as well as experimentally study the effects of stress on transformation, which can provide theoretical bases and mathematical models for numerical simulation. Thus, many investigations in this area have been carried out recently [10–16].

Due to high efficiency and safety, many countries have paid great attention to the development of high-speed trains in recent years. Many research institutions and steel enterprises have conducted research in rail production. The microstructure of the rail steel is pearlite, which is the two-phase mixture of ferrite and cementite. Although the chemical composition of the heavy rail steel for the high-speed train is mostly identical to that of the general rail, the heavy rail for the high-speed train has more strict technical requirements of purity, boundary dimensions, flatness, and heat treatment process. The heavy rail steel needs to be heat treated after hot rolling, in order to improve its mechanical performance to meet the requirements of production. During the heat treatment, the phase transformation of austenite to pearlite occurs. However, there is little research reported on the effects of applied stress on the isothermal phase transformation of austenite to pearlite in heavy rail steels.

In this study, transformation kinetics and transformation plasticity models have been established. The effects of applied stress on transformation kinetics and transformation plasticity have been analyzed. Also, the effects of applied stress on the morphology of the generated pearlite microstructure have been observed by confocal laser scanning microscopy (CLSM) and scanning electron microscopy (SEM).

Materials and Experimental Procedure

The chemical composition of the studied steel is given in Table 1. This steel was preprocessed into cylindrical specimens 6 mm in diameter and 80 mm in height.

The heat treatment experiments were conducted in vacuum on a Gleeble-1500D thermal–mechanical simulator. The specimens were preheated to 900 °C at a heating rate of 10 °C/s and held for 5 min to fully homogenize the microstructure. After that, certain compressive loads, i.e., 0, 20, 30, and 40 MPa, were rapidly applied to the specimens along the axial direction by the Gleeble simulator. The specimens were then cooled to 650 °C at a cooling rate of 10 °C/s and held for 5 min. Since there is no obvious difference between the transformation plasticity under tension and that under compression for the lower applied stress, only compressive loads were applied in this study [16]. Figure 1 shows the schematic diagram of the experimental procedure.

As reported in our previous work [17], the applied axial loads in this study are lower than the yield stress of 47.18 MPa of the studied steel at 900 °C, and the phase transformation of austenite to pearlite can be fully completed within the holding time of 5 min. The variation of

Table 1 Chemical composition of the studied steel (wt%)

C	Si	Mn	P	S	V	Al	Fe
0.750	0.620	0.940	0.019	0.008	0.050	0.005	Bal.

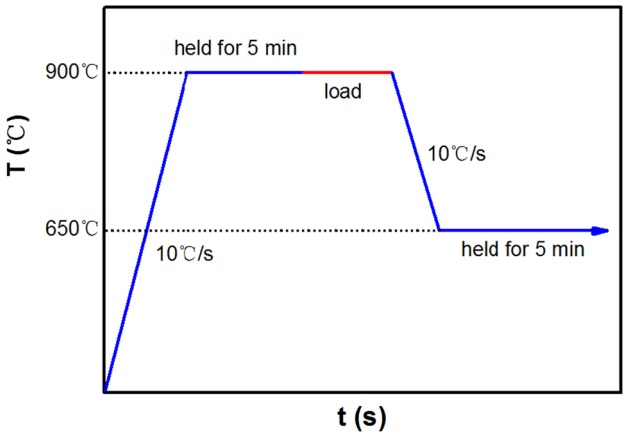

Fig. 1 Schematic diagram of the experimental procedure

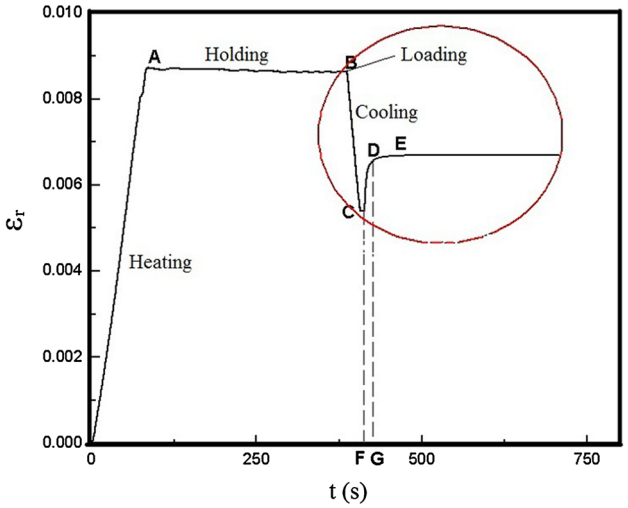

Fig. 2 Relationship between radial strain and time during the entire experimental procedure

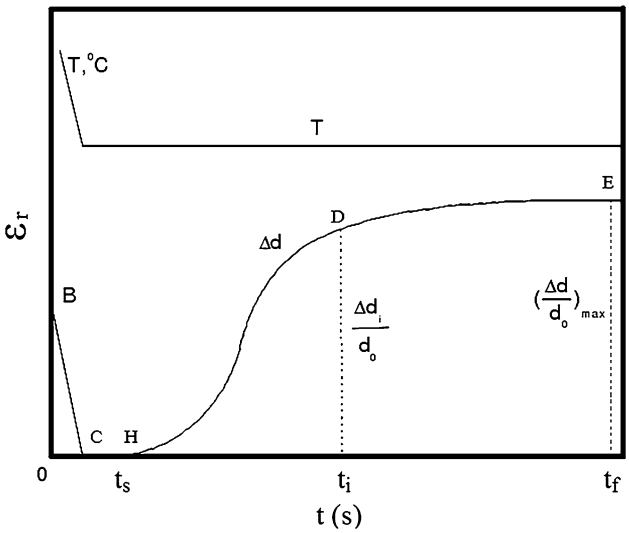

Fig. 3 Schematic diagram of the relationship between radial strain and time during the cooling and transformation process

diameter of the specimens during the whole transformation process was measured and recorded by a dilatometer. The microstructures of the specimens after the experiments were observed by CLSM and SEM.

Modeling the Phase Transformation

Volume Expansion in the Transformation Process

For the reason that austenite is denser than pearlite, during the transformation of austenite to pearlite, the volume of the specimen increases [18–20]. In this study, the two ends of the specimen were constrained by chucks, and thus only radial expansion was measured.

During the transformation process, the radial strain of the studied steel caused by volume expansion can be expressed as:

$$\varepsilon_r = \frac{\Delta d}{d_0} \tag{1}$$

Based on the value of Δd measured during the experiments, the relationship between radial strain and time can be obtained, as shown in Fig. 2. The relationship between radial strain and time during the cooling and transformation process (the red circled area in Fig. 2) is shown in detail in Fig. 3 where t_s and t_f represent the start time and terminal time of transformation, respectively.

In Fig. 2, line 0–A illustrates that the radial strain linearly increases with increasing time in the heating process. A–B is the holding stage in which the radial strain remains almost unchanged. B–C is the cooling stage in which radial strain linearly decreases with increasing time. This indicates that phase transformation does not occur in the cooling stage. C–E is the phase transformation stage in which the transformation of austenite to pearlite occurs. The radial strain increases with increasing time in this stage and then remains unchanged at the end of this stage.

Two cases are discussed below. (1) When not axially loaded, the radial strain C–F only contains thermal strain. Radial strain D–G contains not only thermal strain, but also transformation strain. Since the thermal strains included in C–F and D–G are not produced at the same temperature, the vertical dimension of C–D represents the thermal strain during the phase transformation. (2) When axially loaded, the radial strain C–F contains thermal strain and elastic strain. Radial strain D–G contains not only thermal strain and transformation strain, but also elastic strain and transformation plasticity strain. Therefore, the vertical dimension of C–D represents transformation strain,

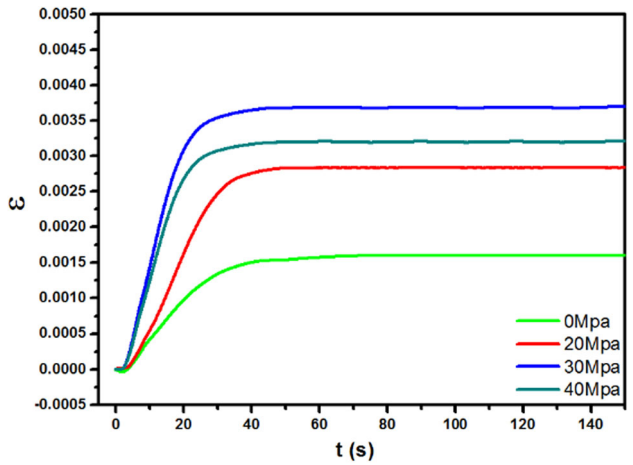

Fig. 4 Relationship between the vertical dimension of C–D and time with different applied stresses

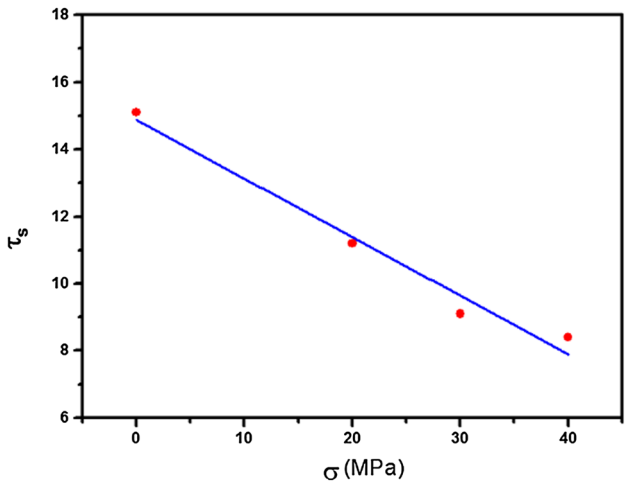

Fig. 5 Relationship between the incubation time and the applied stress

transformation plasticity strain, and corrected elastic strain. Due to the change in elasticity modulus after phase transformation, the elastic strains included in C–F and D–G are not equal to each other, and the difference between the two values is the corrected elastic strain. Therefore, the relationship between the vertical dimension of C–D and time can be obtained, as shown in Fig. 4. Figure 4 shows that the applied stress can significantly decrease the phase transformation time of austenite to pearlite.

Incubation Time for Pearlite Formation

In general, the transformation of austenite to pearlite is unable to start immediately when the austenite is cooled to the transformation temperature. However, the transformation will start after holding for a while, and this time span is regarded as the incubation time [21, 22]. In Fig. 3, the segment C–H illustrates the incubation time in this study.

Figure 5 shows the relationship between the incubation time and the applied stress. Figure 5 shows that when the applied compressive stress increases from 0 to 40 MPa, the incubation time decreases from 15.1 to 8.4 s. This indicates that the applied stress can greatly shorten the incubation time. When transformation of austenite to pearlite occurs at higher temperature, the chemical driving force is low. The applied stress can provide the extra strain energy which can significantly increase the nucleation rate and further shorten the incubation time [21, 22].

As shown in Fig. 5, there is an approximately linear mathematical relationship between the incubation time and the applied stress. Applying a linear fitting method, the following relationship can be obtained:

$$\tau_s = 14.87 - 0.1746\sigma \tag{2}$$

Development of Phase Transformation Kinetics

The isothermal phase transformation of austenite to pearlite kinetics can be expressed by the Avrami equation [23–27]:

$$f = 1 - \exp(-bt^n) \tag{3}$$

If loaded, Eq. (3) needs to be modified to take into consideration the effects of applied loads on phase transformation kinetics.

Determination of b and n in the Original Avrami Equation

When not loaded, radial strain only contains transformation strain:

$$\varepsilon_r = \varepsilon_r^{\mathrm{tr}} = \beta_P^T f \tag{4}$$

When austenite fully transformed into pearlite, $f = 1$ and radial strain reaches its maximum value:

$$\varepsilon_{r\max} = \beta_P^T \tag{5}$$

According to Eqs. (4) and (5), f can be expressed as:

$$f = \frac{\varepsilon_r}{\varepsilon_{r_{\max}}} \tag{6}$$

Taking logarithms on both sides of Eq. (3), Eq. (7) can be obtained:

$$\ln[-\ln(1-f)] = \ln b + n \ln t \tag{7}$$

During the transformation process, radial strain can be measured at different times. Submitting the measured values into Eq. (7), and conducting linear fitting, the values of b and n can be, respectively, calculated as 0.00324 and 1.609.

Transformation Plasticity Model

When loaded, radial strain consists of transformation strain, transformation plasticity strain, and corrected elastic strain, as expressed by:

$$\varepsilon_r = \varepsilon_r^{\mathrm{tr}} + \varepsilon_r^{\mathrm{tp}} + \varepsilon_r^{e'} \tag{8}$$

Transformation strain can be obtained by Eq. (4). According to plastic flow rule of metallic materials [21, 22, 28], radial strain and axial strain have the following relationship:

$$\varepsilon_r^{\mathrm{tp}} = -\upsilon\varepsilon_a^{\mathrm{tp}} = -0.5\varepsilon_a^{\mathrm{tp}} \tag{9}$$

where υ is Poisson's ratio which is the absolute value of the ratio of radial normal strain to axial normal strain, and its value varies with temperature. The value of Poisson's ratio of the studied steel can be found in our previous work [17].

At the beginning of transformation, the microstructure of the studied steel only consists of austenite, and the axial elastic strain of the specimen can be expressed by:

$$\varepsilon_{a,0}^e = \frac{\sigma}{E_A} \tag{10}$$

At the end of transformation, the applied load remains unchanged; however, the elasticity modulus changes due to the phase transformation. Consequently, the axial elastic strain of the specimen changes into:

$$\varepsilon_{a,f}^e = \frac{\sigma}{E_P f + E_A(1-f)} \tag{11}$$

Thus, the increment of the axial elastic strain during the entire transformation process can be calculated by:

$$\Delta\varepsilon^e = \varepsilon_f^e - \varepsilon_0^e = \left[\frac{1}{E_P f + E_A(1-f)} - \frac{1}{E_A}\right]\sigma \tag{12}$$

According to the plastic flow rule of metallic materials [21, 22, 28], the corrected value of the radial elastic strain can be obtained:

$$\varepsilon_r^{e/} = -\upsilon(\Delta\varepsilon_l^e) = \upsilon\left[\frac{1}{E_A} - \frac{1}{E_P f + E_A(1-f)}\right]\sigma \tag{13}$$

The value of elasticity modulus varies with temperature and can be found in our previous work [17].

According to Greenwood and Johnson [29], transformation plasticity results from the density difference between the original and the generated phase. The microstress caused by transformation leads to the occurrence of microscopic plastic strain in the phase with lower strength. If not loaded, the average value of the microscopic plastic strain is approximately zero, and thus only spherical strain occurs at the macroscopic level. If loaded, the microscopic plastic strain in the loading direction cannot be counteracted, and thus the transformation plastic strain occurs at the macroscopic level. The value of the transformation plastic strain is determined by the strength of the phase with lower strength, and it is hardly affected by the orientation effect of the generated phase. In this study, the generated pearlite has little orientation effect. Therefore, the Greenwood–Johnson model is used to describe to transformation plasticity during the phase transformation of austenite to pearlite, as expressed by [29]:

$$\varepsilon_a^{\mathrm{tp}} = K\sigma f(2-f) \tag{14}$$

The value of $\varepsilon_r^{\mathrm{tp}}$ can be obtained by combination of Eqs. (8), (4), and (13). Substituting Eq. (9) into Eq. (14), the transformation plasticity coefficient K can be expressed and calculated by Eq. (15):

$$K = \frac{\varepsilon_a^{\mathrm{tp}}}{\sigma f(2-f)} = \frac{-2(\varepsilon_r)^{\mathrm{tp}}}{\sigma f(2-f)} \tag{15}$$

As a consequence, the transformation plasticity coefficient K under different applied stress can be obtained, as shown in Fig. 6. Figure 6 shows that K increases with increasing applied stress, and there is an approximate linear relationship between them. Conducting linear fitting method shows that this relationship can be expressed by:

$$K = 3.43 \times 10^{-5} + 2.2 \times 10^{-6}\sigma \tag{16}$$

Therefore, the transformation plasticity strain for the studied steel during phase transformation under the experimental conditions can be obtained:

$$\varepsilon_r^{\mathrm{tp}} = -0.5(3.43 \times 10^{-5} + 2.2 \times 10^{-6}\sigma)\sigma f(2-f) \tag{17}$$

Transformation Kinetics

When loaded, the Avrami equation needs to be modified, so as to take the effects of the applied stress on transformation kinetics into account. In the original Avrami equation, the parameters b and n are constants. In this

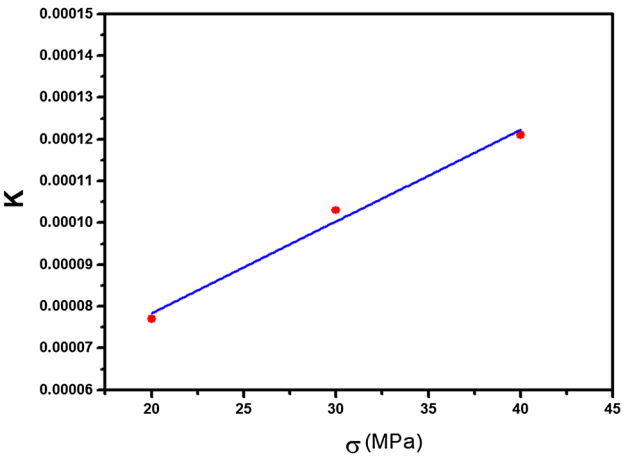

Fig. 6 Relationship between transformation plasticity coefficient and applied stress

study, b and n are changed into variables with the applied stress.

Assuming that $P(f) = \frac{1}{E_A} - \frac{1}{E_P f + E_A(1-f)}$, Eq. (18) can be deduced by second-order Taylor expansion of $P(f)$ under the condition of $f = 1$:

$$P(f) = P(1) + P^{'}(1)(f-1) + o((f-1)) \tag{18}$$

Setting $a_0 = \frac{E_P - E_A}{E_P E_A} - \frac{E_P - E_A}{E_P^2}$ and $a_1 = \frac{E_P - E_A}{E_P^2}$, Eq. (13) can be simplified as:

$$\varepsilon_r^{e'} = \upsilon\sigma(a_0 + a_1 f) \tag{19}$$

According to our previous work [17], a_0 and a_1 can be obtained as 1.013×10^{-7} and 1.076×10^{-6}, respectively.

Substituting Eqs. (4), (14), and (13) into Eq. (8), the following equation can be obtained:

$$\varepsilon_r = \beta_P^T f - \frac{1}{2} K\sigma f(2-f) + \upsilon\sigma(a_0 + a_1 f) \tag{20}$$

Setting $a = \frac{1}{2}K\sigma$, $b = \beta_P^T - K\sigma + \upsilon\sigma a_1$, and $c = \upsilon\sigma a_0 - \varepsilon_r$, f can be expressed as:

$$f = \frac{-b + \sqrt{b^2 - 4a \times c}}{2a} \tag{21}$$

The value of f at different times of transformation can be calculated by Eq. (21), and the value of b and n can be obtained by Eq. (7). The relationship between b/n and applied stress is shown in Figs. 7 and 8. Conducting linear fitting, b and n can be determined as:

$$n = 1.63 + 0.016\sigma \tag{22}$$

$$b = 0.0032 + 1.75 \times 10^{-4}\sigma \tag{23}$$

Verification of the Established Model

The comparison between the measured and the predicted radial strain is shown in Fig. 9. Figure 9 shows that in most cases the predicted data agree well with the measured data, which indicates that the established model has an acceptable accuracy.

Effects of Applied Stress on Phase Transformation

When not loaded, the pearlite volume fraction can be calculated by Eq. (6). When loaded, the pearlite volume fraction can be calculated by Eq. (21). The relationship between pearlite volume fraction and time is shown in Fig. 10.

Figure 10 shows that with the applied stresses of 0, 20, 30, and 40 MPa, when the pearlite fraction reaches 50 %, the required times are 21.66, 16.68, 14.31, and 13.15 s, respectively; when the pearlite fraction reaches 90 %, the required times are 40.10, 35.76, 27.30, and 25.23 s, respectively. This indicates that the applied stress can speed up the transformation of austenite to pearlite.

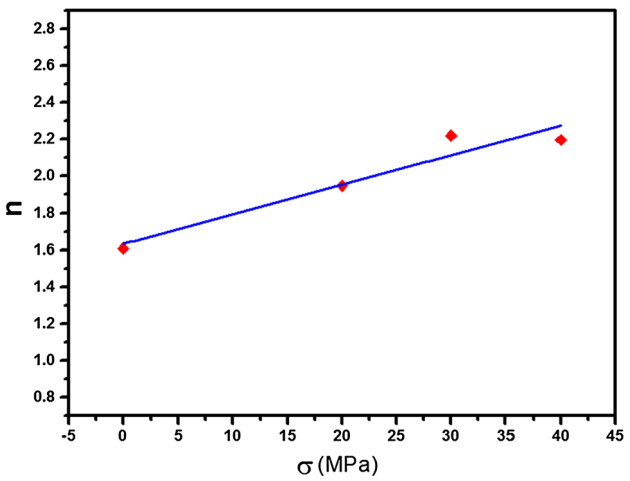

Fig. 7 Relationship between n and applied stress

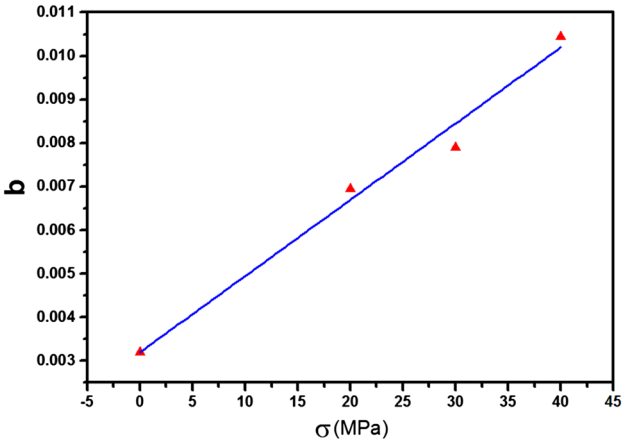

Fig. 8 Relationship between b and applied stress

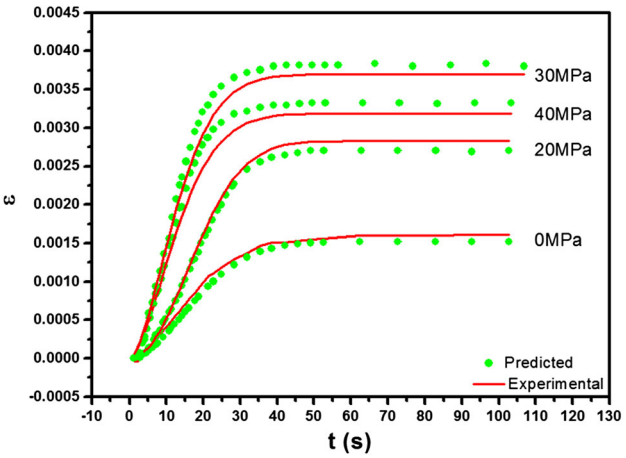

Fig. 9 Comparison between the measured and the predicted radial strain

Besides, the speed-up effect promotes with increasing applied stress.

The microstructures of the specimens after the phase transformation with different applied stresses were respectively observed by CLSM and SEM, as shown in Figs. 11 and 12. When not loaded, the microstructure after transformation mainly consists of lamellar pearlite. When applied stress increases to 20 MPa, globular pearlite becomes noticeable. When applied stress increases to 40 MPa, the fraction of globular pearlite further increases. Globular pearlite is indicated by the presence of very short, globular-shaped lamellae.

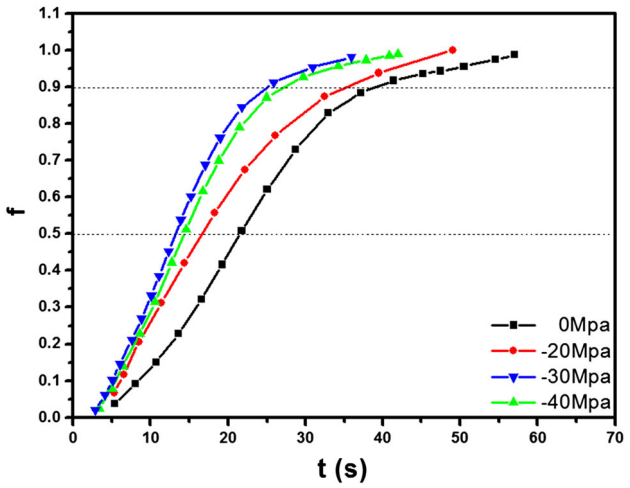

Fig. 10 Relationship between pearlite volume fraction and time

As shown in Fig. 12, when not loaded, the microstructure after phase transformation is regular lamellar pearlite with an interlamellar spacing of 0.452 μm. When loaded with an applied stress of 20 MPa, the microstructure is mostly regular lamellar pearlite, but a small part of globular pearlite. The interlamellar spacing deceases to 0.312 μm. When the applied stress increases to 40 MPa, the microstructure mainly consists of globular pearlite. This suggests that with increasing applied stress, the interlamellar spacing of lamellar pearlite decreases and the fraction of globular pearlite gradually increases. Possibly, the reason is that the stress distribution inside the specimen is nonuniform, which leads to lattice distortion and increasing dislocation density. This further leads to the segregation of carbide. In carbon-rich areas, carbide is easier to

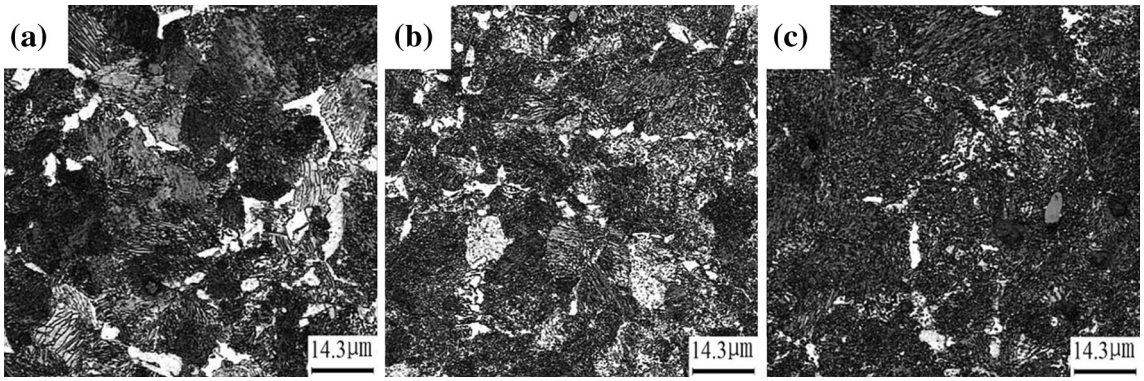

Fig. 11 CLSM figures of the microstructure of the specimens after transformation with different applied stresses of: **a** 0 MPa, **b** 20 MPa, **c** 40 MPa

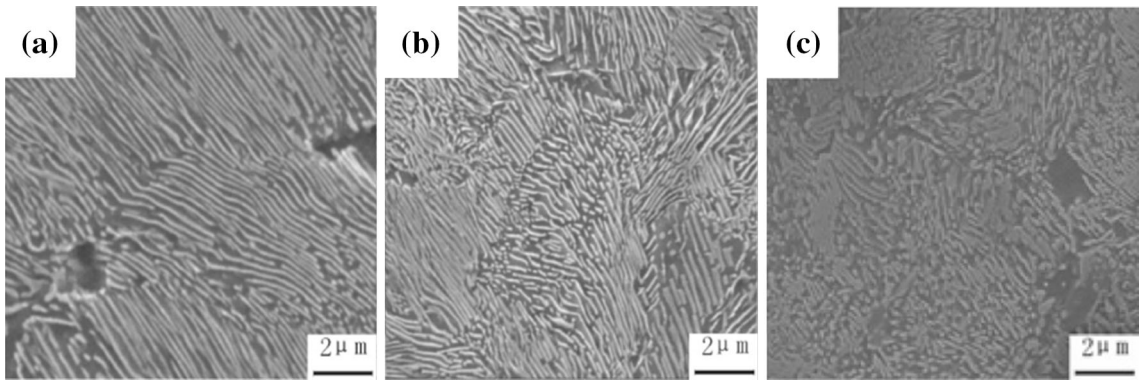

Fig. 12 SEM figures of the microstructure of the specimens after transformation with different applied stresses of: **a** 0 MPa, **b** 20 MPa, **c** 40 MPa

generate, which provides an advantage for the nucleation of globular pearlite. In addition, local stresses near the dislocations and the grain boundaries are likely to be far greater than the applied stress. Although it may not meet the requirement of plastic deformation from a macroscale, the maximum value of the local stress inside the specimen may far exceed the yield stress. Therefore, plastic deformation possibly occurs in this case, causing lattice distortion and an increase in dislocation density. This may also result in the increased nucleation rate of globular pearlite.

Conclusions

In the present study, the effects of applied stress on the isothermal phase transformation of austenite to pearlite in heavy rail steels during heat treatment were analyzed. The following conclusions can be drawn, and these conclusions can be of great use in numerical simulations of heat treatment for heavy rail steels.

1. The applied stress can greatly shorten the incubation time of the phase transformation from austenite to pearlite.
2. The transformation plasticity effect of the studied heavy rail steel during heat treatment was described on the basis of the Greenwood–Johnson mechanism. When the applied stress is lower than the yield stress, the transformation plasticity coefficient K increases with increasing applied stress. The transformation plasticity strain can be expressed as:

$$\varepsilon_r^{tp} = -0.5(3.43 \times 10^{-5} + 2.2 \times 10^{-6}\sigma)\sigma f(2-f)$$

3. A modified Avrami equation was proposed to take the effects of the applied stress on transformation kinetics into account. The transformation kinetics model is:

$$\begin{cases} f = 1 - \exp(-bt^n) \\ n(\sigma) = 1.63 + 0.016\sigma \\ b(\sigma) = 0.0032 + 1.75 \times 10^{-4}\sigma \end{cases}$$

4. With increasing applied stress, the interlamellar spacing of lamellar pearlite decreases and the fraction of globular pearlite gradually increases.

Acknowledgments This work was financially supported by National Natural Science Foundation of China. (No. 51361021), the Major Project of Natural Science Foundation of Inner Mongolia Autonomous Region (No. 2012ZD09), and the Scientific Research Project of the Inner Mongolia Autonomous Region Higher Education (No. NJZZ12099).

References

1. J. Mackerle, Finite element analysis and simulation of quenching and other heat treatment processes: a bibliography (1976–2001). Comput. Mater. Sci. **27**, 313–332 (2003)
2. M. Yaakoubi, M. Kchaou, F. Dammak, Simulation of Heat treatment and materials with the use of the Abaqus software. Met. Sci. Heat Treat. **55**, 386–392 (2013)
3. S. Eck, P. Prevedel, S. Marsoner et al., Using finite element simulation to optimize the heat treatment of tire protection chains. J. Mater. Eng. Perform. **23**, 1288–1295 (2014)
4. F. Bubani, M. Sade, V. Torra et al., Stress induced martensitic transformations and phases stability in Cu–Al–Be shape-memory single crystals. Mater. Sci. Eng., A **583**, 129–139 (2013)
5. V. Levitas, I. Ozsoy et al., Micromechanical modeling of stress-induced phase transformations. Part 1. Thermodynamics and kinetics of coupled interface propagation and reorientation. Int. J. Plast **25**, 239–280 (2009)
6. H. Huang, Y. Wang, J. Xie, Stress-induced phase transformation characteristics and its effect on the enhanced ductility in continuous columnar-grained polycrystalline Cu–12 wt% Al alloy. Mater. Sci. Eng., A **596**, 103–111 (2014)
7. F. Fischer, G. Reisner, G. Werner et al., A new view on transformation induced plasticity. Int. J. Plast **16**, 723–740 (2000)
8. A. Tahimi, F. Barbe, L. Taleb et al., Evaluation of microstructure-based transformation plasticity models from experiments on 100C6 steel. Comput. Mater. Sci. **52**, 55–60 (2012)
9. T. Inoue, T. Tanaka, D. Ju et al., Transformation plasticity and the effect on quenching process simulation. Key Eng. Mater. **345–346**, 915–918 (2007)
10. M. Fischlschweiger, E. Oberaigner, Kinetics and rates of martensitic phase transformation based on statistical physics. Comput. Mater. Sci. **52**, 189–192 (2012)
11. H. Zong, T. Lookman, X. Ding et al., The kinetics of the ω to α phase transformation in Zr, Ti: analysis of data from shock-recovered samples and atomistic simulations. Acta Mater. **77**, 191–199 (2014)
12. H. Bok, S. Kim, D. Suh et al., Non-isothermal kinetics model to predict accurate phase transformation and hardness of 22MnB5 boron steel. Mater. Sci. Eng., A **626**, 67–73 (2015)
13. M. Gómez, S. Medina, G. Caruana, Modelling of phase transformation kinetics by correction of dilatometry results for a ferritic Nb-microalloyed steel. ISIJ Int. **43**, 1228–1237 (2003)
14. H. Zhao, X. Liu, G. Wang, Progress in modeling of phase transformation kinetics. J. Iron. Steel Res. Int. **13**, 68–73 (2006)
15. S. Rajasekhara, P. Ferreira, Martensite-austenite phase transformation kinetics in an ultrafine-grained metastable austenitic stainless steel. Acta Mater. **59**, 738–748 (2011)
16. H. Zhao, S. Lee, Y. Lee et al., Effects of applied stresses on martensite transformation in AISI4340 Steel. J. Iron. Steel Res. Int. **14**, 63–67 (2007)
17. G. Chang, Effects of low stress on transformation plasticity and microstructure in heavy rail steels, Master thesis, Inner Mongolia University of Science and Technology, Baotou, 2014
18. M. Aranda, B. Kim, R. Rementeria et al., Effect of prior austenite grain size on pearlite transformation in a hypoeuctectoid Fe–C–Mn Steel. Metall. Mater. Trans. A **45**, 1778–1786 (2014)
19. C. Verdi, A. Visintin, A mathematical model of the austenite-pearlite transformation in plain carbon steel based on the Scheil's additivity rule. Acta Metall. **35**, 2711–2717 (1987)
20. S. Offerman, L. Wilderen, N. Dijk et al., Cluster formation of pearlite colonies during the austenite/pearlite phase transformation in eutectoid steel. Phys. B **335**, 99–103 (2003)

21. H. Bhadeshia, Physical Metallurgy of Steels, in *Physical Metallurgy*, 5th edn., ed. by D. Laughlin, K. Hono (Elsevier B.V, Amsterdam, 2014), pp. 2157–2214
22. R. Smallman, A. Ngan, *Modern Physical Metallurgy*, 8th edn. (Elsevier B.V, Amsterdam, 2014)
23. J. Wang, H. Kou, H. Chang et al., Limitation of the Johnson-Mehl-Avrami equation for the kinetic analysis of crystallization in a Ti-based amorphous alloy. Int. J. Miner. Metall. Mater. **17**, 307–311 (2010)
24. A. Pietak, M. Sayer, M. Stott, Crystallization kinetics of Si-TCP bioceramic films. J. Mater. Sci. **39**, 2443–2449 (2004)
25. J. Jonas, X. Quelennec, L. Jiang et al., The Avrami kinetics of dynamic recrystallization. Acta Mater. **57**, 2748–2756 (2009)
26. H. Luo, Effect of concurrent recovery on Avrami exponent of the softening kinetics after hot deformation. Mater. Sci. Eng., A **532**, 44–49 (2012)
27. J. Kohout, Modelling of changes in properties of alloys at elevated temperatures. Mater. Sci. Eng., A **462**, 159–163 (2007)
28. W. Hosford, *Mechanical Behavior of Materials, 2ed* (Cambridge University Press, Cambridge, 2010)
29. G. Greenwood, R. Johnson, The deformation of metals under small stresses during phase transformations. Proc. R. Soc. A-Math. Phys. Eng. Sci. **283**, 403–422 (1965)
30. L. Taleb, F. Sidoroff, A micromechanical modeling of the Greenwood-Johnson mechanism in transformation induced plasticity. Int. J. Plast **19**, 1821–1842 (2003)